Title: 2-Carboxyquinoxalines kill *Mycobacterium tuberculosis* through non-covalent inhibition of DprE1

Authors:

João Neres,[1,2*] Ruben C. Hartkoorn,[1,2*] Laurent R. Chiarelli,[1,3*] Ramakrishna Gadupudi,[4,5*] Maria Rosalia Pasca,[1,3] Giorgia Mori,[1,3] Davide Farina,[5] Svetlana Savina,[1,6] Vadim Makarov,[1,6] Gaelle S. Kolly,[1,2] Elisabetta Molteni,[1,3] Claudia Binda,[1,3] Neeraj Dhar,[1,2] Stefania Ferrari,[4,5] Priscille Brodin,[1,7] Vincent Delorme,[1,7] Valérie Landry,[7] Ana Luisa de Jesus Lopes Ribeiro,[3^] Alberto Venturelli,[4] Puneet Saxena,[5] Florence Pojer,[1,2] Antonio Carta,[8] Rosaria Luciani,[5] Alessio Porta,[9] Giuseppe Zanoni,[9] Edda De Rossi,[1,3] Maria Paola Costi,[1,4,5§] Giovanna Riccardi,[1,3§] Stewart T. Cole[1,2§]

Affiliations:

[1] More Medicines for Tuberculosis (MM4TB) Consortium (www.mm4tb.org),

[2] Global Health Institute, Ecole Polytechnique Fédérale de Lausanne, 1015 Lausanne, Switzerland,

[3] Department of Biology and Biotecnology "Lazzaro Spallanzani", University of Pavia, 27100 Pavia, Italy,

[4] Tydock Pharma srl Via Campi 183, 41125 Modena, Italy,

[5] Department of Life Sciences, University of Modena and Reggio Emilia, Via Campi 183, 41126 Modena, Italy

[6] A. N. Bakh Institute of Biochemistry, Russian Academy of Science, 119071 Moscow, Russia,

[7] Inserm U1019 – CNRS UMR 8204, Institut Pasteur de Lille, Université de Lille, 1 rue du Professeur Calmette, 59019, Lille, France,

[8] Department of Chemistry and Pharmacy, University of Sassari, 07100 Sassari, Italy,

[9] Department of Chemistry, University of Pavia, 27100 Pavia, Italy.

^ Present address: Centro de Biologia Molecular "Severo Ochoa" Universidad Autónoma de Madrid, 28049, Madrid, Spain

*These authors contributed equally to the work

§To whom correspondence should be addressed: stewart.cole@epfl.ch (S.T.C), giovanna.riccardi@unipv.it (G.R.) , hcostimp@unimore.it (M.P.C)

Abstract: Phenotypic screening of a quinoxaline library against replicating *Mycobacterium tuberculosis* led to the identification of lead compound Ty38c (3-((4-methoxybenzyl)amino)-6-(trifluoromethyl)quinoxaline-2-carboxylic acid). With an MIC_{99} and MBC of 3.1 μM, Ty38c is bactericidal and active against intracellular bacteria. To investigate its mechanism of action we isolated mutants resistant to Ty38c and sequenced their genomes. Mutations were found in *rv3405c*, coding for the transcriptional repressor of the divergently expressed *rv3406* gene. Biochemical studies clearly showed that Rv3406 decarboxylates Ty38c into its inactive keto metabolite. The actual target was then identified by isolating Ty38c-resistant mutants of an *M. tuberculosis* strain lacking *rv3406*. Here, mutations were found in *dprE1*, encoding the decaprenylphosphoryl-D-ribose oxidase DprE1, essential for biogenesis of the mycobacterial cell wall. Genetics, biochemical validation, and X-ray crystallography revealed Ty38c to be a non-covalent, non-competitive DprE1 inhibitor. Structure-activity relationship studies generated a family of DprE1 inhibitors with a range of IC_{50}s and bactericidal activity. Co-crystal structures

of DprE1 in complex with eight different quinoxaline analogs provided a high-resolution interaction map of the active site of this extremely vulnerable target in *M. tuberculosis*.

INTRODUCTION

More than 130 years after Koch's discovery of *Mycobacterium tuberculosis* as its etiological agent, tuberculosis (TB) still affects humankind and was responsible for 1.3 million deaths in 2012 [1, 2]. This disease reemerged in recent decades as an increasingly important public health problem due to the appearance of multidrug resistant (MDR-TB) and extensively drug resistant (XDR-TB) strains with high mortality rates, the synergy with the HIV/AIDS pandemic and increased poverty [1, 3, 4]. After decades of relative inactivity in TB drug discovery, a promising pipeline of TB drug candidates in different stages of development has emerged recently [5]. In 2012, bedaquiline, the first new TB drug approved since the 1960s, brought new hope for many patients with MDR-TB [6]. Several molecules are now in preclinical studies, phase II and III clinical trials, but the pipeline still needs more novel scaffolds to provide backup drugs given the high attrition rate observed during clinical development [5, 7]. Phenotypic screens have emerged as an efficient means of identifying active compounds for TB drug discovery, especially as almost all hits from target-based screens, which provided potent enzyme inhibitors failed to display useful bactericidal activity against *M. tuberculosis* [8].

Here, we report the discovery of a family of quinoxalines with antitubercular activity, following a phenotypic screen of a chemical library against replicating *M. tuberculosis*. The lead compound Ty38c (3-((4-methoxybenzyl)amino)-6-(trifluoromethyl)quinoxaline-2-carboxylic acid) is active against extracellular and intracellular *M. tuberculosis*. We have elucidated both a mechanism of resistance to Ty38c and its mechanism of action, and validated the findings using

biochemical assays and X-ray crystallography. Furthermore, the synthesis and structure activity relationship studies of analogs of Ty38c provide valuable information regarding this novel DprE1 inhibitor scaffold.

RESULTS AND DISCUSSION

A phenotypic screen identifies a tuberculocidal quinoxaline scaffold

Single point screening of a library containing 266 quinoxaline analogs against *M. tuberculosis* H37Rv using the resazurin reduction assay revealed five compounds with MIC_{99} <15 μM. In order to focus on non-nitroaromatic scaffolds, with potentially novel mechanisms of action, we selected a 2-carboxyquinoxaline cluster with 3 compounds: Ty38c, Ty21c (the ethyl ester of Ty38c) and Ty36c (Table 1). Ty38c and Ty21c killed intracellular H37Rv in a macrophage model with IC_{50}s of 2.5 and 6.1 μM, respectively. Both compounds were inactive against the non-replicating ss18b *M. tuberculosis* strain (MIC_{99} >100 μM), suggesting that they inhibit a function essential for growth. Ty38c and Ty21c presented selectivity indexes (TD_{50}/MIC_{99}) of 12 and 15, respectively, based on their HepG2 cytotoxicity (Table 1). Ty38c was confirmed to be bactericidal with an MBC equal to its MIC_{99} of 3.1 μM (1.2 μg/ml). Cidality was also directly visualized using microfluidics-based time-lapse microscopy of *M. tuberculosis* expressing GFP [9]. Exposure of H37Rv to 5 μM Ty38c caused a dramatic reduction in the growth rate of individual bacteria (Fig. 1, Movie Supplementary Movie 1), although some cells continued to divide without elongation. Cell lysis occurred after a certain lag (25-30 h), and most of the cells lysed over the 7-day exposure period.

Rv3406 is responsible for primary resistance of *M. tuberculosis* to Ty38c

To identify the molecular target(s) of Ty38c, we isolated spontaneous resistant mutants of *M. tuberculosis* H37Rv; these arose at a frequency of $1x10^{-6}$ on solid medium containing 20 μM Ty38c, and their Ty38c-resistance profile was confirmed in liquid culture (Supplementary Table 2). Whole-genome sequencing and bioinformatics analysis of four independent mutants (TRC1 - TRC4) revealed that each mutant carried a different non-synonymous single nucleotide polymorphism (SNP) or a single base deletion in the *rv3405c* gene (Supplementary Table 2). This gene codes for a transcriptional regulator of the TetR family. Sanger sequencing of *rv3405c* confirmed the mutations in these four mutants and in six additional independently isolated Ty38c-resistant mutants (TRC5 – TRC10; Supplementary Table 2).

The *rv3405c* gene is expressed divergently from the neighboring *rv3406* gene encoding an iron and α-ketoglutarate (α-KG) dependent sulfate ester dioxygenase, which oxidizes medium-chain alkyl-sulfate esters like 2-ethylhexyl sulfate (2-EHS, Fig. 2A) [10]. Interestingly, a unique palindrome (TGTAGTCAtcTGACTACA) is found between *rv3405c* and *rv3406* that could represent the DNA binding sequence of *rv3405c*. Quantitative Real-Time PCR (qRT-PCR) experiments confirmed that the Ty38c-resistant mutants (TRC5 and TRC6), have significantly increased transcription of *rv3406* (30- and 47.2-fold respectively), as well as *rv3405c* itself (15.7-fold increase) (Supplementary Table 3). This therefore suggests that Rv3405c is a transcriptional repressor controlling both *rv3405c* and *rv3406* and that mutations in Rv3405c lead to their overexpression, in agreement with a recent report in *M. bovis* BCG [11].

To confirm that overexpression of Rv3406 causes Ty38c resistance, *rv3405c* or *rv3406* were cloned into a pSODIT-2 expression vector, the resultant plasmids were transformed into H37Rv and the susceptibility of selected transformants to Ty38c determined (Supplementary Table 4). Compared to H37Rv:pSODIT (MIC_{99} 2.5 μg/ml), the data clearly showed that

overexpression of *rv3406* in H37Rv:pSODIT/*rv3406* conferred an >8-fold increase in resistance to Ty38c (MIC_{99} >20 µg/ml), whereas H37Rv:pSODIT/*rv3405c* showed the same susceptibility to Ty38c as H37Rv:pSODIT. Importantly, transformation of pSODIT/*rv3405c* into the Ty38c-resistant mutant TRC5 complemented the resistance phenotype of TRC5 (MIC_{99} 2.5-5 µg/ml) compared to the vector control (MIC_{99} >20 µg/ml). This confirmed that mutations in Rv3405c prevent transcriptional repression of *rv3406*, and that Rv3406 overexpression leads to Ty38c resistance.

Rv3406 inactivates Ty38c

To understand the putative resistance mechanism caused by Rv3406, we expressed and purified this protein (Supplementary Fig. 1). The activity of the recombinant Rv3406 enzyme was followed by the rate of oxygen consumption using α-KG and 2-EHS as substrates (Table 2). First, we tested whether Ty38c (up to 250 µM) could inhibit Rv3406 in standard assay conditions, but this was not the case. We then determined whether Ty38c could replace either αKG or 2-EHS as a substrate and be metabolized by the enzyme. Rv3406 was enzymatically active in the presence of Ty38c and 2-EHS (in the absence of α-KG), but not when incubated with Ty38c and α-KG in the absence of EHS, showing that Rv3406 can use Ty38c instead of α-KG as a substrate. Subsequent kinetic analysis showed that Ty38c presents a 14-fold lower k_{cat} value and a 17-fold higher K_m value as compared to α-KG (Table 2), indicating that Rv3406 metabolizes Ty38c significantly less efficiently than α-KG in the assay conditions. We isolated and purified the reaction products from the reaction mixture, and through NMR and mass spectrometry, the main metabolite was identified as a keto derivative of Ty38c (QN113), resulting from oxidative decarboxylation by Rv3406 (Fig. 2B). In parallel, we independently

synthesized and characterized QN113 and thus confirmed the metabolite's identity (see Supporting Information). QN113 was inactive against wild-type H37Rv and the TRC5 mutant (MIC_{99} > 40 μg/ml). Together, the data clearly demonstrate that resistance results from decarboxylative inactivation of Ty38c by Rv3406 *in vitro* and most likely in *M. tuberculosis* as well, following derepression of the *rv3406* gene.

To obtain structural information regarding the mode of binding of Ty38c to Rv3406 and potentially use a structure-based approach to design improved Ty38c analogs that avoid decarboxylation, we attempted to obtain crystal structures of the complex. However, only crystals of native Rv3406 protein with bound Fe^{2+} were obtained, which diffracted to 2.0 Å (Supplementary Fig. 2 and Supplementary Table 7).

DprE1 is the target of Ty38c

To find the actual target of Ty38c, responsible for its anti-mycobacterial activity, we constructed H37RvΔ*rv3406*, an H37Rv strain lacking Rv3406, by recombineering [12], and confirmed the correct replacement of *rv3406* with a hygromycin cassette by PCR. The susceptibility of H37RvΔ*rv3406* to Ty38c was identical to that of wild type H37Rv. We then isolated spontaneous Ty38c-resistant mutants in H37RvΔ*rv3406*, which arose at a much lower frequency ($1x10^{-8}$) than was seen with H37Rv. Two mutants (TRC11 and TRC12) showed 4-fold resistance to Ty38c, but were as susceptible to moxifloxacin as wild-type H37Rv. Whole genome sequencing revealed two different non-synonymous SNPs in the *dprE1* gene (g49t and t1103c, translating to G17C and L368P, respectively). No cross-resistance was observed between either of these *dprE1* mutants and the prototypic DprE1 inhibitor BTZ043, but mutations that result in resistance to benzothiazinones (NTB1 mutant, C387S [13]) conferred cross-resistance to Ty38c (4-

fold increase in MIC_{99}). These data suggested that Gly17, Leu368 and Cys387 are involved in Ty38c binding.

Additional genetic validation of DprE1 as the target of Ty38c was performed using a conditional expression system in *M. tuberculosis*, in which *dprE1* is overexpressed following addition of pristinamycin. Over-expression of *dprE1* caused a >16-fold increase in resistance to both BTZ043 and Ty38c, whilst not affecting susceptibility to the control drug (Supplementary Table 5).

Biochemical assays using recombinant *M. tuberculosis* DprE1, and the G17C and L368P mutant enzymes were used to assess enzyme inhibition. As previously reported for *M. smegmatis* DprE1 [14], the *M. tuberculosis* enzyme presents non-Michaelis-Menten behavior, with a sigmoidal-shaped initial velocity *versus* substrate concentration curve, so the data were fitted to the Hill equation [15]. The G17C and L368P mutants presented $K_{0.5}$ values similar to the wild type enzyme, but were 34- and 6.6-fold less efficient, respectively, based on the determined k_{cat} values (Table 3). Ty38c effectively inhibited wild-type DprE1 with an IC_{50} of 41 nM and behaved as a non-competitive inhibitor, with a K_i of 25.9 nM. The G17C and L368P mutants were significantly less susceptible to Ty38c, with IC_{50} values of 0.15 and 1.3 μM, respectively (Table 3), in agreement with the MIC_{99} determined against the corresponding Ty38c-resistant H37Rv*Δrv3406 dprE1* mutants.

SAR studies on Ty38c reveal key features required for DprE1 inhibition

Given the potency of Ty38c and the novelty of this scaffold as an antitubercular agent, we pursued Structure-Activity Relationship (SAR) studies to improve it and understand the substituent requirements needed to achieve DprE1 inhibition and activity against *M.*

184 *tuberculosis*, whilst trying to avoid inactivation by Rv3406. SAR studies focused on the 2-
185 carboxylate, the 6-trifluoromethyl and the 3-benzylamine moieties (synthesis described in the
186 Supporting Information). All Ty38c analogs were tested in biochemical assays as substrates for
187 Rv3406 or inhibitors of DprE1 (Tables 4, 5 and Supplementary Table 6), and for their activity
188 against *M. tuberculosis* H37Rv, its *rv3405c* (TRC4) and Δ*rv3406* DprE1 mutants (G17C and
189 L368P), and against intracellular H37Rv in the macrophage model of infection.

190 Compounds designed to resist the activity of Rv3406, where the 2-carboxylate group was
191 replaced by a methyl group (QN106, QN107, QN108 and QN109) or by a carboxamide (QN102,
192 QN104, QN103 and QN105), were not active against *M. tuberculosis* and showed only residual
193 inhibition of DprE1 (Table 4). As mentioned above, the keto analogue QN113 was inactive
194 against DprE1. Interestingly, some of the 2-carboxyl ethyl esters (Tables 4 and Supplementary
195 Table 6), namely Ty21c, QN101, QN144 and QN141, presented reasonable MIC_{99} against *M.*
196 *tuberculosis* H37Rv (3.1-12.5 μM), but none was significantly active against DprE1 ($IC_{50} \geq 50$
197 μM). These results indicate that the esters' activity against the bacterium is likely due to
198 hydrolysis to the free acid, during the long incubation period in culture medium, or to the action
199 of mycobacterial esterases.

200 Absence of the 6-trifluoromethyl moiety in quinoxalines QN111, QN110 and QN112
201 (Table 4), led to near complete loss of whole cell activity ($MIC_{99} \geq 50$ μM) and DprE1 inhibition
202 (IC_{50} between 16 and 33 μM) but did not prevent decarboxylation by Rv3406, with turnover
203 rates between 0.35 and 0.62 min^{-1}.

204 In the 2-carboxy-6-trifluoromethyl-quinoxaline series (Table 6) there was significant
205 modulation of the various parameters tested depending on the modifications introduced in
206 position 3 of the quinoxaline ring. A benzyl group (present in Ty38c) is preferred to a phenyl in

this position (QN131 versus Ty38c), likely due to the flexibility introduced by the methylene spacer, which may improve interaction with the active site of DprE1. QN130, a synthetic intermediate lacking the benzyl moiety was not active. The remaining eighteen Ty38c analogs had benzyl groups with varied substitution patterns (Table 5). The best compounds in this series, with an MIC_{99} of 3.1 μM, were Ty38c, QN114 and QN124, which had single substitutions in the *para* position of the benzene ring (OMe, OEt and Cl, respectively), and were also among the most potent DprE1 inhibitors (IC_{50}s of 0.041 - 0.088 μM). Minor modifications on the benzyl group were not favorable, leading to a 2- to 16-fold increase in MIC_{99} (e.g.: replacing the methoxy group by methyl, fluoro, trifluoromethyl or nitrile (Ty38c *versus* QN119, Ty36c, QN127 or QN129, respectively) . However, these compounds retained DprE1 inhibition (IC_{50}s of 0.072 - 0.12 μM), implying that they might not reach the target as efficiently in the bacterium. Compounds with a single substituent in the *meta* position, or with double substitutions in the *meta* and *para* positions showed a significant increase in MIC_{99} accompanied by a drop in potency against DprE1 (Table 5).

A modest positive correlation ($R^2 = 0.21$) was found between MIC_{99} values and DprE1 inhibition for the Ty38c analogs modified in the 3-benzyl moiety (Table 5 and Supplementary Fig. 3A). All compounds in this series were decarboxylated by Rv3406, with rates varying between 0.08 min^{-1} for QN122 to 1.19 min^{-1} for Ty36c. These data shows that modifications in the substituent in position 3 of the quinoxalines can effectively modulate the Rv3406-substrate ability. Importantly, there was no correlation between MIC_{99} values and Rv3406 activity (Supplementary Fig. 3B) and Ty38c, the compound with the lowest MIC_{99}, was also the best substrate for Rv3406. Therefore, despite playing a role in the development of resistance to the 2-carboxyquinoxalines *in vitro*, Rv3406 does not seem to significantly affect their antitubercular

activity against exponentially growing wild type *M. tuberculosis* probably due to its repression mediated by Rv3405c.

The SAR data presented above shows that the 6-trifluoromethyl-2-carboxyquinoxalines with a *para*-substituted benzyl group in position 3 are the best compounds at inhibiting DprE1, and at killing *M. tuberculosis in vitro*. All compounds displayed 2-fold higher MIC_{99} against a selected *rv3405c* mutant compared to H37Rv and, in most cases, the MIC_{99} increased 4-fold against the G17C and L368P DprE1 mutants (TRC11 and TRC12, respectively). Good MIC_{99} *in vitro* did not always translate into activity against intracellular bacteria, as only Ty38c and Ty21c were bactericidal intracellularly, with IC_{50} values in the same range as their MIC_{99}. This fact underlines the importance of evaluating compounds not only against *M. tuberculosis* in culture but also in infected host cells, to have a complete view of their potential efficacy *in vivo*. All the modified benzyl analogs of Ty38c showed IC_{50}s between 41 and 220 nM, hence this moiety has the potential to accommodate substantial modifications in order to improve stability, cytotoxicity or even to prevent inactivation by Rv3406.

Ty38c and analogs interact with key residues in the active site of DprE1

To understand the SAR data at a structural level, we co-crystallized *M. tuberculosis* DprE1 with several Ty38c analogs. Complexes with eight quinoxalines (Ty38c, Ty21c, QN114, Ty36c, QN118, QN124, QN127 and QN129) were obtained, diffracting to 1.8 - 2.5 Å, with crystals in the space group previously found for the PBTZ169 complex[16] (Supplementary Table 7). Co-crystallization attempts with analogs lacking the 2-carboxylate or the 6-CF_3 groups generally led to good quality crystals that displayed no electron density for the compounds in the active site of DprE1.

The overall structure of DprE1 in the quinoxaline complexes was identical to that of previously reported structures [14, 17, 18]. The two loops that were disordered in most available DprE1 structures are resolved to different extents in the new complexes. While the 267-298 loop is fully resolved in monomer A of almost all structures, electron density was observed for the whole 315-329 loop in only two cases (Ty36c and QN129 complexes), providing important clues regarding the flexibility and potential interactions of these residues with the 2-carboxyquinoxalines. This loop could also be involved in interactions with the cell membrane or with other protein partners involved in the DPA biosynthetic pathway [14, 19]. Residue Tyr314, which when mutated to a histidine leads to resistance to TCA1 [18] and other reported non-covalent DprE1 inhibitors (Supplementary Fig. 7), is located at the edge of this loop and close to the active site, but does not interact with the quinoxalines presented here.

In all complexes, the common 2-carboxy-6-trifluoromethylquinoxaline core is invariably observed in the same position, next to the FAD flavin ring, with an angle of 22° between the planes defined by the two ring systems (Fig. 3). The trifluoromethyl group is located in a small hydrophobic pocket formed by His132, Gly133, Lys367, Lys134, Ser228 and Phe369, as previously observed for the same group in BTZ043 or PBTZ169 [14, 16]. Key hydrogen bonds are formed between the side-chain of Lys418, an essential catalytic residue [14], and the carboxylate group and nitrogen 1 of the quinoxaline ring. The hydroxyl group of Tyr60 also forms a hydrogen bond with the carboxylate. In the Ty36c and QN129 complexes, the 315-329 loop seems to be stabilized by an extra electrostatic interaction between the side-chain of Arg325 and the quinoxaline's carboxylate. However, this loop presents high B-factors, and adopts alternative conformations in other DprE1-quinoxaline complexes (Supplementary Fig. 4).

Major differences were observed in the mode of binding of the benzyl moiety of Ty38c and its analogs (Fig. 3A-D). In monomer B, these inhibitors were always present in a bent conformation, the planes defined by the quinoxaline and benzene rings being approximately perpendicular in the various structures (Fig. 3C and 3D). The benzene ring is placed near the side chain of Leu363 and induces a conformational change of the side-chain of Trp230 compared to previously published structures. In monomer A, the situation varied between inhibitors: QN124, QN127 and QN129 adopt the bent conformation (identical to that observed in monomer B), Ty38c, Ty36c and QN114 are present in a planar conformation (benzyl and quinoxaline rings approximately co-planar), and QN101 is apparently in two populations of bent and co-planar conformations (Fig. 3A and 3B). In the planar conformation, the benzyl group is surrounded by the side-chains of Leu317, Asn324 and Arg325.

Interestingly, when the compound was present in the bent conformation in monomer A, extra electron density was observed in its vicinity (Fig. 3E), and here we modeled a tri-propylene-glycol (tri-PG) molecule, as poly-propylene glycol is present in the crystallization conditions. Following refinement, the modeled tri-PG molecule presented average B-factors of 59 - 75 $Å^2$, compared to 40 - 45 $Å^2$ for the inhibitors in the same monomer. The tri-PG was located between the quinoxaline ring and residues Pro316, Leu363, Trp230, Ala244, Ser246 and Ser228, in approximately the same location where extra electron density was found in the DprE1 complex with PBTZ169 [16], and this pocket may correspond to the binding site of the DPR substrate of DprE1.

In addition, a co-crystal structure of Ty21c (ethyl ester of Ty38c) was obtained, in which electron density was clearly observed in the active site of monomer A (Supplementary Fig. 5B). The structure was refined after fitting Ty38c here, bound in the same manner as in the DprE1-

Ty38c complex (Supplementary Figs. 5A and 5B). No electron density to account for the ethyl moiety of the ester was observed, which could have undergone hydrolysis according to our hypothesis discussed above.

Gly17 and Leu368, mutated to Cys and Pro, respectively in DprE1 in Ty38c-resistant mutants do not interact directly with the quinoxaline inhibitors (Figs. 3A, 3C, Supplementary Figs. 6A and 6B). Gly17 is located near Tyr60 (Supplementary Fig. 6A), therefore a mutation to a cysteine might induce conformational adjustments affecting the interaction of this residue with the carboxylate of the inhibitors. A Leu368Pro mutation could affect adjacent residues, including Lys367, part of the trifluoromethyl binding pocket (Supplementary Fig. 6B), eventually interfering with binding of Ty38c and its analogs.

Overall, despite substantial structural differences when compared to the benzothiazinones, the quinoxalines occupy approximately the same space in the active site as BTZ043 or PBTZ169, and the non-covalent inhibitor TCA1 (Fig. 3F). The main difference between PBTZ169 and the quinoxaline family of inhibitors resides in the absence of the covalent bond with Cys387 for the quinoxalines, which seems to be compensated, in part, by strong electrostatic interactions between Lys418 and Arg325, and the carboxylate group.

CONCLUSIONS

A change in the TB drug discovery paradigm in recent years led to a move away from target-based screens to whole-cell screens [20]. Surprisingly, despite the use of distinct chemical libraries with broad chemical diversity, many of the hit compounds were found to inhibit a very limited number of targets in mycobacteria. Examples of these “promiscuous targets”, inhibited by a

range of structurally unrelated molecules, are the trehalose monomycolate transporter MmpL3 (targeted by compounds SQ109, AU1235, BM212 and C215 among others) and DprE1[5].

DprE1 is a highly vulnerable and fully validated TB drug target, essential for the decaprenylphosphoarabinose (DPA) pathway, crucial for cell wall biosynthesis and mycobacterial growth [21-23]. BTZ043 and PBTZ169, among the most potent TB drug candidates discovered so far (MIC_{99} of 1 and 0.3 ng/ml, respectively), are suicide, covalent inhibitors of DprE1[14b, 18]; PBTZ169 is expected to enter clinical trials in the near future [16]. An impressive range of eight compound scaffolds with antitubercular activity has been recently shown to target DprE1 as covalent or non-covalent inhibitors (Supplementary Fig. 7).

Here, we report a new family of DprE1 inhibitors, the 2-carboxy-6-trifluoromethylquinoxalines, discovered in a whole-cell screen, and disclose initial SAR data. The best compound Ty38c exhibits strong activity against replicating *M. tuberculosis in vitro* as well as in macrophages. Target finding for Ty38c was not straightforward. Spontaneous resistant mutants of *M. tuberculosis* to Ty38c presented mutations in Rv3405c, which controls expression of *rv3406* [11]. Rv3406 is an α-ketoglutarate-dependent sulfate ester dioxygenase of broad substrate specificity [10], which decarboxylates Ty38c to an inactive keto metabolite. The decarboxylating activity of Rv3406 on aromatic carboxylates reported here could prove important for other potential antitubercular drugs with carboxyl groups, which might undergo similar inactivation.

To find the actual target of Ty38c, we constructed a H37Rv*Δrv3406* knock-out mutant and used this to generate new Ty38c-resistant mutants, which contained *dprE1* point mutations. DprE1 was then confirmed as the target of Ty38c by genetic and biochemical means. The most

potent Ty38c analogs displayed IC_{50}s <100 nM, and Ty38c was found to be a non-competitive inhibitor of DprE1, with a K_i of 25.9 nM.

SAR studies on the Ty38c scaffold, supported by crystallographic data, have shown that the carboxylate group forms crucial electrostatic and hydrogen bond interactions with Lys418, Tyr60 and possibly Arg325. The 6-trifluoromethyl group of Ty38c seems to be optimal for binding. Position 3 in the quinoxaline ring was found to be more amenable to modifications. Interestingly, the 3-benzyl group in these compounds mimics the cyclohexylmethylpiperazine moiety of PBTZ169 (Fig. 5D), which was found to accommodate various modifications and fully retain MIC against *M. tuberculosis*. These moieties in Ty38c and PBTZ169 have a hydrophobic character and project towards the exposed surface of the protein and so they might also interact with protein partners of DprE1, or with the cell membrane. Importantly, the apparent lack of specific interactions of the benzyl group in Ty38c offers the opportunity to introduce structural changes in order to improve potency and ADME/T properties.

A major strength of the present work is the richness of the high-resolution structural data presented for DprE1 in complex with a variety of 2-carboxyquinoxaline derivatives. Combined with previous structural information [14, 16-18], a detailed model of the various interactions possible between small molecule inhibitors and the active site of the enzyme can now be generated. This interaction map is extended by two new positions in DprE1 that modulate quinoxaline binding, Gly17 and Leu368. The apparent promiscuity of DprE1 in binding a large range of chemical scaffolds might be attributable to the space available close to the FAD flavin ring, which is then able to form stacking interactions with various heterocyclic ring systems, thereby occluding part of the expected substrate binding site. In addition, the flexibility of the 315-329 loop, located immediately above the active site cavity, may also favor access of compounds to the active site

and thus account for the large range of scaffolds. Furthermore, the association of DprE1 with the cell membrane should facilitate access to more hydrophobic inhibitors [24]. The wealth of new structural insight obtained in the present study will underpin structure-based drug design of DprE1 inhibitors.

METHODS

Synthesis of Ty38c and analogs

Ty38c and its derivatives were synthesized through the adaptation of previously published procedures [25]. Synthetic routes, experimental details and compound characterization data are provided in the Supporting Information.

Library-screening

A library of 266 quinoxaline analogs was screened at the concentration of 20 μM for anti-tuberculosis activity on log-phase *M. tuberculosis* H37Rv using the resazurin reduction assay (REMA) [26]. Compounds that showed >80% inhibition of H37Rv growth were subsequently analyzed for their minimal inhibitory concentrations (MIC_{99}) against log phase H37Rv, non-replicating ss18b [27, 28]; intracellular activity against H37Rv [29] and cytotoxicity against the human hepatocellular carcinoma cell line, HepG2. The minimum bactericidal activity (MBC) of the lead compound, Ty38c, was then determined using a colony forming unit (cfu) inhibition assay.

Rv3406 enzymatic assays and steady state kinetics

The enzymatic activity of Rv3406 was determined by measuring the rate of oxygen consumption with a Hansatech Oxygraph oxygen electrode, using α-ketoglutarate (αKG) and 2-ethylhexylsulfate (2-EHS) as substrates, at 25°C with atmospheric oxygen. The standard reaction mixture contained 20 mM imidazole pH 7.0, 0.05 mM 2-EHS, 0.5 mM αKG, 0.1 mM $FeSO_4$, 0.2 mM sodium ascorbate, in a final volume of 1 ml, and the reaction was started by adding enzyme solution (5 μM).

Steady-state kinetics parameters were determined as follows: for α-KG and Ty38c at fixed concentration of 0.05 mM 2-EHS; for 2-EHS at 0.5 mM α-KG. In all cases the reaction was started by addition of the enzyme and activity assayed at >8 different substrate concentrations. All experiments were performed in duplicate, and the kinetic constants, K_m and k_{cat}, were determined fitting the data to the Michaelis-Menten equation using Origin 8 software. Rv3406 activity towards Ty38c analogs was determined in triplicate, using 0.2 mM of each compound. The metabolite resulting from the inactivation of Ty38c by Rv3406 was isolated following incubation with the enzyme at 37°C for 5 hours (details in Supporting Information).

DprE1 inhibition assays

DprE1 assays were performed on the *M. tuberculosis* enzyme, in black 96-well half-area plates (Corning 3686), in a final volume of 30 μl. DprE1 (300 nM), FAD (1 μM), Horseradish peroxidase (2 μM, Sigma-Aldrich P-6782) and Amplex Red (50 μM, Life Technologies A-22177) in 50 mM glycylglycine pH 8.0, 200 mM potassium glutamate and 0.002% Brij-35 was incubated at 30°C with the test compound (DMSO stock, final conc.: 1%) for 10 min, followed by the addition of farnesyl-phosphoryl-β-D-ribofuranose (FPR) to 300 μM. The conversion of Amplex Red to resorufin was followed by fluorescence measurement (excitation/emission:

560/590 nm) on a Tecan M200, in kinetic mode, at 30°C. A negative control with no inhibitor was used, and the background rate (no added FPR) subtracted from measured rates. Fluorescence units were converted to resorufin concentration using a calibration curve in assay buffer. Kinetic constants were calculated using Prism (GraphPad Software). Steady-state kinetic constants were determined by fitting data to the Hill equation (Equation 1) [15]. IC_{50} values were determined by fitting log[I] and normalized response to Equation 2, and the K_i for Ty38c was determined using an adapted equation for non-competitive inhibition of enzymes with sigmoidal behavior (Equation 3).

$$V = \frac{V_{max} \times [S]^h}{(K_{0.5})^h + [S]^h} \qquad \textbf{Equation 1}$$

$$V = \frac{100}{\{1 + 10^{(\log(IC_{50} - [I]) \times h)}\}} \qquad \textbf{Equation 2}$$

$$V = \frac{\frac{V_{max}}{\left(1 + \frac{I}{K_i}\right)} \times [S]^h}{(K_{0.5})^h + [S]^h} \qquad \textbf{Equation 3}$$

DprE1 crystallization and structure determination. Crystals of *M. tuberculosis* DprE1 in complex with Ty38c, Ty36c, Ty21c, QN127, QN124, QN129, QN118 and QN114 were obtained by the hanging-drop vapor diffusion method at 18°C. One or 0.5 µL of DprE1 (7 mg/ml) in 20 mM Tris pH 8.0, 100 mM NaCl and 0.7 mM of the carboxyquinoxaline (DMSO stock, final conc.: 7%), was mixed with 1 µl of the reservoir solution containing 100 mM imidazole pH 6.9-7.5 and 34-39% polypropyleneglycol 400. Yellow crystals grew in approximately 1-3 days and were transferred to a cryo-protectant (reservoir solution with 25% glycerol) prior to, or frozen directly by flash-cooling in liquid nitrogen. X-ray data were collected at the X06DA beamline of the Swiss Light Source synchrotron (Villigen). Data processing and scaling are described in the Supporting Information.

Accession Codes: Coordinates and structure factors for the crystal structures here reported have been deposited in the Protein Database with access code 4CVY for Rv3406, and the following codes for the DprE1 complexes: 4P8K (Ty38c), 4P8L (Ty36c), 4P8M (QN114), 4P8N (QN118), 4P8P (QN124), 4P8C (QN127), 4P8T (QN129) and 4P8Y (Ty21c).

REFERENCES AND NOTES:

1. *Global TB Report 2013*; WHO: Geneva, Switzerland, 2013.
2. Migliori, G. B.; Loddenkemper, R.; Blasi, F.; Raviglione, M. C., 125 years after Robert Koch's discovery of the tubercle bacillus: the new XDR-TB threat. Is "science" enough to tackle the epidemic? *Eur. Respir. J.* **2007,** *29*, 423-427.
3. Green, K.; Garneau-Tsodikova, S., Resistance in tuberculosis: what do we know and where can we go? *Frontiers Microbiol.* **2013,** *4*, 208.
4. Koul, A.; Arnoult, E.; Lounis, N.; Guillemont, J.; Andries, K., The challenge of new drug discovery for tuberculosis. *Nature* **2011,** *469*, 483-490.
5. Zumla, A.; Nahid, P.; Cole, S. T., Advances in the development of new tuberculosis drugs and treatment regimens. *Nature Rev. Drug Discov.* **2013,** *12*, 388-404.
6. Diacon, A. H.; Pym, A.; Grobusch, M.; Patientia, R.; Rustomjee, R.; Page-Shipp, L.; Pistorius, C.; Krause, R.; Bogoshi, M.; Churchyard, G.; Venter, A.; Allen, J.; Palomino, J. C.; De Marez, T.; van Heeswijk, R. P. G.; Lounis, N.; Meyvisch, P.; Verbeeck, J.; Parys, W.; de Beule, K.; Andries, K.; Mc Neeley, D. F., The Diarylquinoline TMC207 for Multidrug-Resistant Tuberculosis. *N. Engl. J. Med.* **2009,** *360*, 2397-2405.

7. Lechartier, B.; Rybniker, J.; Zumla, A.; Cole, S. T., Tuberculosis drug discovery in the post-post-genomic era. *EMBO Mol. Med.* **2014,** *6*, 158-68.

8. Sala, C.; Hartkoorn, R. C., Tuberculosis drugs: new candidates and how to find more. *Future Microbiol.* **2011,** *6*, 617-633.

9. Wakamoto, Y.; Dhar, N.; Chait, R.; Schneider, K.; Signorino-Gelo, F.; Leibler, S.; McKinney, J. D., Dynamic Persistence of Antibiotic-Stressed Mycobacteria. *Science* **2013,** *339*, 91-95.

10. Sogi, K. M.; Gartner, Z. J.; Breidenbach, M. A.; Appel, M. J.; Schelle, M. W.; Bertozzi, C. R., Mycobacterium tuberculosis Rv3406 Is a Type II Alkyl Sulfatase Capable of Sulfate Scavenging. *Plos One* **2013,** *8*, e65080

11. Galvão, T. C.; Lima, C. R.; Ferreira Gomes, L. H.; Pagani, T. D.; Ferreira, M. A.; Gonçalves, A. S.; Correa, P. R.; Degrave, W. M.; Mendonca-Lima, L., The BCG Moreau RD16 deletion inactivates a repressor reshaping transcription of an adjacent gene. *Tuberculosis* **2014,** *94*, 26-33.

12. van Kessel, J. C.; Hatfull, G. F., Recombineering in Mycobacterium tuberculosis. *Nature Methods* **2007,** *4*, 147-152.

13. Makarov, V.; Manina, G.; Mikusova, K.; Moellmann, U.; Ryabova, O.; Saint-Joanis, B.; Dhar, N.; Pasca, M. R.; Buroni, S.; Lucarelli, A. P.; Milano, A.; De Rossi, E.; Belanova, M.; Bobovska, A.; Dianiskova, P.; Kordulakova, J.; Sala, C.; Fullam, E.; Schneider, P.; McKinney, J. D.; Brodin, P.; Christophe, T.; Waddell, S.; Butcher, P.; Albrethsen, J.; Rosenkrands, I.; Brosch, R.; Nandi, V.; Bharath, S.; Gaonkar, S.; Shandil, R. K.; Balasubramanian, V.; Balganesh, T.; Tyagi, S.; Grosset, J.; Riccardi, G.; Cole, S. T., Benzothiazinones Kill Mycobacterium tuberculosis by Blocking Arabinan Synthesis. *Science* **2009,** *324*, 801-804.

14. Neres, J.; Pojer, F.; Molteni, E.; Chiarelli, L. R.; Dhar, N.; Boy-Roettger, S.; Buroni, S.; Fullam, E.; Degiacomi, G.; Lucarelli, A. P.; Read, R. J.; Zanoni, G.; Edmondson, D. E.; De Rossi, E.; Pasca, M. R.; McKinney, J. D.; Dyson, P. J.; Riccardi, G.; Mattevi, A.; Cole, S. T.; Binda, C., Structural Basis for Benzothiazinone-Mediated Killing of Mycobacterium tuberculosis. *Science Translat. Med.* **2012,** *4*, 150ra121.

15. Copeland, R. A., *Enzymes: A practical introduction to structure, mechanism and data analysis*. 2nd ed.; John Wiley & Sons Inc.: New York, NY, 2000.

16. Makarov, V.; Lechartier, B.; Zhang, M.; Neres, J.; van der Sar, A.; Raadsen, S.; Hartkoorn, R.; Ryabova, O.; Vocat, A.; Decosterd, L.; Widmer, N.; Buclin, T.; Bitter, W.; Andries, K.; Pojer, F.; Dyson, P.; Cole, S., Towards a new combination therapy for tuberculosis with next generation benzothiazinones. *EMBO Mol. Med.* **2014,** *6*, 372-83.

17. Batt, S. M.; Jabeen, T.; Bhowruth, V.; Quill, L.; Lund, P. A.; Eggeling, L.; Alderwick, L. J.; Fuetterer, K.; Besra, G. S., Structural basis of inhibition of Mycobacterium tuberculosis DprE1 by benzothiazinone inhibitors. *P.N.A.S.* **2012,** *109*, 11354-11359.

18. Wang, F.; Sambandan, D.; Halder, R.; Wang, J.; Batt, S. M.; Weinrick, B.; Ahmad, I.; Yang, P.; Zhang, Y.; Kim, J.; Hassani, M.; Huszar, S.; Trefzer, C.; Ma, Z.; Kaneko, T.; Mdluli, K. E.; Franzblau, S.; Chatterjee, A. K.; Johnson, K.; Mikusova, K.; Besra, G. S.; Futterer, K.; Jacobs, W. R., Jr.; Schultz, P. G., Identification of a small molecule with activity against drug-resistant and persistent tuberculosis. *P.N.A.S.* **2013,** *110*, E2510-7.

19. Mikusova, K.; Huang, H. R.; Yagi, T.; Holsters, M.; Vereecke, D.; D'Haeze, W.; Scherman, M. S.; Brennan, P. J.; McNeil, M. R.; Crick, D. C., Decaprenylphosphoryl arabinofuranose, the donor of the D-arabinofuranosyl residues of mycobacterial arabinan, is

497 formed via a two-step epimerization of decaprenylphosphoryl ribose. *J. Bact.* **2005,** *187*, 8020-
498 8025.
499 20. Payne, D. J.; Gwynn, M. N.; Holmes, D. J.; Pompliano, D. L., Drugs for bad bugs:
500 confronting the challenges of antibacterial discovery. *Nature Rev. Drug Discov.* **2007,** *6*, 29-40.
501 21. Mikusova, K.; Makarov, V.; Neres, J., DprE1 - from the discovery to the promising
502 Tuberculosis drug target. *Curr. Pharm. Des.* **2014,** *20*, 4379-4403.
503 22. Riccardi, G.; Pasca, M. R.; Chiarelli, L. R.; Manina, G.; Mattevi, A.; Binda, C., The
504 DprE1 enzyme, one of the most vulnerable targets of Mycobacterium tuberculosis. *Appl.*
505 *Microbiol. Biotechnol.* **2013,** *97*, 8841-8848.
506 23. Wolucka, B. A., Biosynthesis of D-arabinose in mycobacteria - a novel bacterial pathway
507 with implications for antimycobacterial therapy. *FEBS J.* **2008,** *275*, 2691-2711.
508 24. Goldman, R. C., Why are membrane targets discovered by phenotypic screens and
509 genome sequencing in Mycobacterium tuberculosis? *Tuberculosis* **2013,** *93*, 569-588.
510 25. Corona, P.; Vitale, G.; Loriga, M.; Paglietti, G., Quinoxaline chemistry. Part 13: 3-
511 carboxy-2-benzylamino substituted quinoxalines and N- 4- (3-carboxyquinoxalin-2-yl)
512 aminomethyl benzoyl -L-glutamates: synthesis and evaluation of in vitro anticancer activity.
513 *Farmaco* **2000,** *55*, 77-86.
514 26. Palomino, J. C.; Martin, A.; Camacho, M.; Guerra, H.; Swings, J.; Portaels, F., Resazurin
515 microtiter assay plate: Simple and inexpensive method for detection of drug resistance in
516 Mycobacterium tuberculosis. *Antimicrob. Ag. Chemother.* **2002,** *46*, 2720-2722.
517 27. Sala, C.; Dhar, N.; Hartkoorn, R. C.; Zhang, M.; Ha, Y. H.; Schneider, P.; Cole, S. T.,
518 Simple Model for Testing Drugs against Nonreplicating Mycobacterium tuberculosis.
519 *Antimicrob. Ag. Chemother.* **2010,** *54*, 4150-4158.

28. Zhang, M.; Sala, C.; Hartkoorn, R. C.; Dhar, N.; Mendoza-Losana, A.; Cole, S. T., Streptomycin-Starved Mycobacterium tuberculosis 18b, a Drug Discovery Tool for Latent Tuberculosis. *Antimicrob. Ag. Chemother.* **2012,** *56*, 5782-5789.

29. Christophe, T.; Jackson, M.; Jeon, H. K.; Fenistein, D.; Contreras-Dominguez, M.; Kim, J.; Genovesio, A.; Carralot, J.-P.; Ewann, F.; Kim, E. H.; Lee, S. Y.; Kang, S.; Seo, M. J.; Park, E. J.; Skovierova, H.; Pham, H.; Riccardi, G.; Nam, J. Y.; Marsollier, L.; Kempf, M.; Joly-Guillou, M.-L.; Oh, T.; Shin, W. K.; No, Z.; Nehrbass, U.; Brosch, R.; Cole, S. T.; Brodin, P., High Content Screening Identifies Decaprenyl-Phosphoribose 2 ' Epimerase as a Target for Intracellular Antimycobacterial Inhibitors. *Plos Pathogens* **2009,** *5*, e1000645.

Acknowledgments:

We thank S. Boy-Röttger and P. Busso for technical support, A. Jones for critical reading of the manuscript, the Protein Crystallography Core Facility of EPFL, the Swiss Light Source for beam time and excellent support during X-ray data collection. The research leading to these results received funding from the European Community's Seventh Framework Programme (Grant 260872). P. Brodin was supported by an ERC-STG grant from the European Commission (INTRACELLTB Grant n° 260901), the Agence Nationale de Recherche, the Feder (12001407 (D-AL) Equipex Imaginex BioMed) and the Region Nord Pas de Calais.

ASSOCIATED CONTENT

Supporting Information: Supplementary movies, tables, figures, methods, and references. This material is available free of charge via the Internet at http://pubs.acs.org.

543

544 **Table 1**. Biological profile of the five confirmed hits in the quinoxaline library screening.

	Structure	H37Rv MIC_{99} (μM)	Intracellular activity IC_{50} (μM)	HepG2 cytotoxicity TD50 (μM)
Ty38c	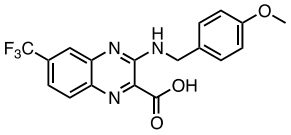	3.1	2.5	37
Ty21c	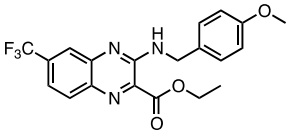	3.1	6.1	48
Ty36c	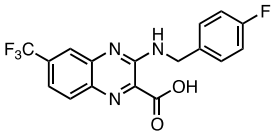	12.5	>20	25

545

546

547 **Table 2.** Kinetic analysis of the enzymatic activity of *M. tuberculosis* Rv3406.

Substrate	K_m (mM)	k_{cat} (min^{-1})	k_{cat}/K_m (min^{-1} mM^{-1})
α-KG [a]	0.0094 ± 0.0012	21.8 ± 1.0	2319 ± 106
Ty38c [a]	0.16 ± 0.01	1.54 ± 0.08	9.6 ± 0.3
2-EHS [b]	0.0088 ± 0.0005	19.2 ± 0.9	2186 ± 97

548 [a] assays were performed at a concentration of 0.05 mM 2-EHS. [b] The kinetic

549 analysis for 2-EHS was performed at a concentration of 0.5 mM α-KG.

550

551

552 **Table 3.** Enzymatic characterization and Ty38c inhibition of *M. tuberculosis* DprE1 wild type,
553 G17C and L368P mutants.

	Wild type	G17C	L368P
$K_{0.5}$ [a] (mM)	242 ± 8	311 ± 20	308 ± 13
h [a]	2.6 ± 0.2	2.6 ± 0.4	3.3± 0.4
k_{cat} (min^{-1}) [b]	4.1 ± 0.6	0.12 ± 0.01	0.62 ± 0.02
IC_{50} Ty38c (µM)	0.041	0.15	1.3
K_i (µM)	0.0259	n.d. [c]	n.d.

554 [a] Data were fitted to the Hill equation for enzymes with sigmoidal behavior; [b] The enzyme
555 concentration in the assay was 0.3, 1.5 and 1.2 µM for the wild type, G17C and L368P
556 mutants, respectively; [c] n.d.: not determined.

557

558

559 **Table 4.** Biological and biochemical characterization of Ty38c analogs with modifications in

560 positions 2 and 6 of the quinoxaline ring.

Compound	Structure					MIC$_{99}$ (μM)			Rv3406 rate [a] (min^{-1})	DprE1 inhibition IC$_{50}$ (μM) or % inhibition at 50 μM
	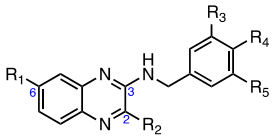					H37Rv	H37Rv *rv3405c* mutant TRC4	H37Rv *Δrv3406 dprE1* L368P		
	R$_1$	**R$_2$**	**R$_3$**	**R$_4$**	**R$_5$**					
Ty38c	CF_3	COOH	H	OMe	H	3.1	6.3	12.5	1.07	0.041
Ty21c	CF_3	COOEt	H	OMe	H	3.1	6.3	12.5-25	0.09	(54%)
QN101	CF_3	COOEt	H	OEt	H	6.3-12.5	12.5	>100	0.07	n.i. [b]
QN102	CF_3	$CONH_2$	H	OMe	H	>100	>100	>100	0.04	n.i.
QN103	CF_3	$CONH_2$	H	CF_3	H	>100	>100	>100	0.03	n.i.
QN104	CF_3	CONHMe	H	OMe	H	>100	>100	>100	0.02	n.i.
QN105	CF_3	CONHMe	H	CF_3	H	>100	>100	>100	0.02	n.i.
QN106	CF_3	Me	H	OMe	H	100	100	100	0	22
QN107	CF_3	Me	OMe	OMe	H	>100	>100	>100	0	20
QN108	CF_3	Me	OMe	OMe	OMe	>100	>100	>100	0	(49%)
QN109	CF_3	Me	H	CF_3	H	100	100	100	0	n.i.
QN110	H	COOH	H	OMe	H	100	>100	100	0.62	23
QN111	H	COOH	OMe	OMe	H	>100	>100	>100	0.35	33
QN112	H	COOH	H	F	H	50-100	100	50-100	0.56	16
QN113	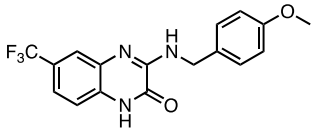					>100	>100	>100	0	n.i.

561 [a] Rv3406 rate determined at 200 μM of the test compound, and calculated by dividing the measured enzyme velocity

562 by the enzyme concentration; [b] n.i.: no inhibition.

563

564

565

Table 5. Biological and biochemical characterization of Ty38c analogs on the 3-benzyl moiety.

Compound	Structure			MIC$_{99}$ (μM)			Rv3406 rate [a] (min^{-1})	DprE1 inhibition IC_{50} (μM) or % inhibition at 50 μM
	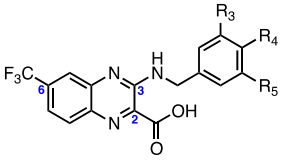			H37Rv	H37Rv *rv3405c* mutant TRC4	H37Rv *Δrv3406 dprE1* L368P		
	R_3	R_4	R_5					
Ty38c	H	OMe	H	3.1	6.3	12.5	1.07	0.041
QN114	H	OEt	H	3.1	6.3	12.5	0.26	0.088
QN115	OMe	OMe	H	50	100	100	0.67	0.16
QN116	OMe	OMe	OMe	100	>100	100	0.33	0.20
QN117	OMe	H	H	25	50	50	0.28	0.083
QN118	F	OMe	H	6.3-12.5	12.5	25	0.22	0.080
QN119	H	Me	H	12.5	12.5-25	25-50	0.38	0.10
QN120	Me	H	H	25	25-50	50	0.17	0.22
QN121	Me	F	H	6.3	12.5	25	0.25	0.13
Ty36c	H	F	H	12.5	25	25	1.19	0.072
QN122	F	H	H	25-50	50	50	0.08	0.16
QN123	F	F	H	25	25-50	50-100	0.27	0.15
QN124	H	Cl	H	3.1	12.5	25	0.21	0.050
QN125	Cl	H	H	25	50-100	50-100	0.25	0.13
QN126	Cl	Cl	H	12.5-25	12.5	25-50	0.27	0.11
QN127	H	CF_3	H	6.3	12.5	25	0.2	0.12
QN128	CF_3	H	H	12.5	25	50	0.17	0.16
QN129	H	CN	H	50	50	100	0.26	0.067
QN130	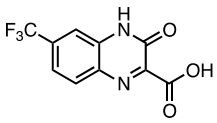			>100	>100	>100	0.05	(40%)
QN131	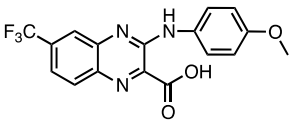			12.5-25	50	50	0.84	0.22

[a] Rv3406 rate determined at 200 μM of the test compound, and calculated by dividing the measured enzyme velocity by the enzyme concentration.

571

572 **FIGURE LEGENDS:**

573 **Fig. 1.** Single-cell analysis of bactericidal activity of Ty38c. *M. tuberculosis* expressing GFP was
574 grown in a microfluidics device and exposed to 5 μM Ty38c between days 5-12. Imaging
575 was carried out at 1-hour intervals during 18 days on fluorescence (FITC) and phase
576 channels. Representative time-series snapshots of an imaged XY-point in the microfluidic
577 device are shown. The medium conditions are indicated on top left (7H9 - no drug;
578 Ty38c). Days are indicated on top right. The scale bar shown at bottom left represents 5
579 μm.

580

581 **Fig. 2.** Reactions catalyzed by Rv3406. (**A)** Oxidation of α-KG by Rv3406 in the presence of 2-
582 EHS leads to the formation of succinate and 2-ethylhexanal. (**B)** Oxidation of Ty38c and
583 its analogs by Rv3406 in the same conditions leads to the decarboxylation of the
584 compound, affording the respective keto derivative.

585

586 **Fig. 3.** Crystal structures of DprE1 in complex with Ty38c and analogs. (**A)** Active site with
587 Ty36c bound in a planar conformation (monomer A in the asymmetric unit). (**B)**
588 Superposed structures of Ty38c and six analogs, in the conformation observed in
589 monomer A. The inhibitor QN118 presented two alternative conformations in this
590 monomer. **(C)** Active site with Ty36c bound in a bent conformation (monomer B), with
591 the disordered loop (316-331) represented by a dashed line. Gly17 and Leu368
592 (represented as spheres), when mutated to Cys and Pro, respectively, confer resistance.
593 The residues forming the pocket where the trifluoromethyl group is bound are shown as a

semi-transparent surface. (**D)** Superposed structures of Ty38c and six analogs, in the conformations observed in monomer B. **(E)** $2F_o$-F_c electron density map contoured at 1.0 RMSD (0.2291 e/Å^3) for QN124 and tri-propylene-glycol (tri-PG), showing the surrounding residues in the DprE1-QN124 complex. (**F)** Superposition of the DprE1 active site-bound conformations of PBTZ169 (PDB 4NCR (*10*)), TCA1 (PDB 4KW5 (*19*)) and Ty38c.